Model calculations of electron precipitation induced ionization patches on the nightside of Mars

M. O. Fillingim,[1] L. M. Peticolas,[1] R. J. Lillis,[1] D. A. Brain,[1] J. S. Halekas,[1]
D. L. Mitchell,[1] R. P. Lin,[1] D. Lummerzheim,[2] S. W. Bougher,[3] and D. L. Kirchner[4]

Received 16 March 2007; revised 2 May 2007; accepted 15 May 2007; published 16 June 2007.

[1] Using an electron transport model, we investigate the effect of electron precipitation on the electron density and total electron content in the nightside ionosphere of Mars. As input we use Mars Global Surveyor observations of a typical tail electron spectrum and an auroral-like electron spectrum. The accelerated electron spectrum increases the maximum number density and total electron content by a factor of 3 over that produced by the typical tail spectrum. Our calculations show a secondary electron density peak due to precipitation of several keV electrons not seen in previous modeling efforts. Regions of enhanced ionization are expected to be localized in space, corresponding to magnetic cusps formed by the interaction of crustal sources with the interplanetary magnetic field. Radio and radar measurements from both Mars Global Surveyor and Mars Express agree with this expectation. The horizontally inhomogeneous regions of ionization can affect signals used for subsurface sounding from orbit. **Citation:** Fillingim, M. O., L. M. Peticolas, R. J. Lillis, D. A. Brain, J. S. Halekas, D. L. Mitchell, R. P. Lin, D. Lummerzheim, S. W. Bougher, and D. L. Kirchner (2007), Model calculations of electron precipitation induced ionization patches on the nightside of Mars, *Geophys. Res. Lett.*, *34*, L12101, doi:10.1029/2007GL029986.

1. Introduction

[2] Mars lacks a global magnetic field, but it does have intense and localized crustal fields yielding a complex magnetic topology [*Acuña et al.*, 2001]. Where the crustal field has a nearly radial orientation, there is a tendency for the field lines to connect with the IMF, forming cusps that provide a conduit for ionospheric plasma to escape and for solar wind plasma to precipitate into the atmosphere [*Mitchell et al.*, 2001]. On the nightside one expects ionization due to solar wind electron precipitation in regions of open (radial) field lines at cusps and an absence of ionization in closed (horizontal) field regions.

[3] Knowledge of the nighttime ionosphere at Mars comes mainly from radio and radar measurements. Several radio occultation (RO) profiles were obtained by Mars 4 and 5 [*Savich et al.*, 1976] and Viking 1 and 2 [*Zhang et al.*, 1990] that indicated peak electron densities of $\sim 5 \times 10^3$ cm^{-3} between altitudes of 110 km and 160 km for solar zenith angles (SZA) of 110° to 130°. Using near-terminator RO measurements from Mars Global Surveyor (MGS), *Withers et al.* [2005] reported anomalous electron density profiles containing "bumps" and "bite-outs" indicative of sharp vertical or horizontal changes in electron density located above crustal magnetic anomalies. Radar soundings of the ionosphere by the Mars Advanced Radar for Subsurface and Ionosphere Sounding (MARSIS) aboard Mars Express (MEX) have shown the presence of significant ionospheric structure on both the dayside [*Gurnett et al.*, 2005; *Duru et al.*, 2006] and nightside (SZA >100°) [*Kirchner et al.*, 2006, 2007] associated with regions of strong vertical crustal magnetic fields.

[4] Particle measurements can give an indication of how the Martian nightside ionosphere is formed. Several authors have modeled the expected nightside ionospheric electron density due to the precipitation of electrons measured at high altitude (~10,000 km) by Phobos 2 [*Verigin et al.*, 1991; *Haider et al.*, 1992; *Fox et al.*, 1993; *Haider*, 1997] and at low altitude (400 km) by MGS [*Haider et al.*, 2002]. Since plasma transport from the dayside can be a major contributor to the nightside ionosphere of Venus, *Fox et al.* [1993] also investigated the role of plasma transport from the dayside as a source of the nightside ionosphere of Mars. Recently, auroral-like peaked electron distributions traveling toward the atmosphere have been observed on the nightside of Mars by MGS [*Brain et al.*, 2006] and MEX [*Lundin et al.*, 2006]. The spatial distribution of accelerated spectra is quite patchy, tending to clump around the perimeter of strong closed field regions [*Brain et al.*, 2006]. Recent work by *Leblanc et al.* [2006] was the first to consider the effect of these accelerated electrons on the atmosphere; however, their work focused on modeling auroral emissions and did not address the resulting change in the ionospheric electron density.

[5] Here we present model calculations of the change in the nightside ionospheric density due to electron precipitation using two different incident spectra as input: a typical tail spectrum and an auroral-like accelerated spectrum. Both of these spectra were observed by MGS at 400 km altitude with nearly radial magnetic field orientations. We compare our calculations with observations and previous calculations of the nightside ionospheric electron density. Finally we discuss the consequences of localized patches of enhanced ionization in the nightside Martian ionosphere.

2. Methodology

[6] To model the electron transport in the Martian atmosphere, we use a modification of the code of *Lummerzheim*

[1]Space Sciences Laboratory, University of California, Berkeley, California, USA.
[2]Geophysical Institute, University of Alaska, Fairbanks, Alaska, USA.
[3]Department of Atmospheric, Oceanic and Space Sciences, University of Michigan, Ann Arbor, Michigan, USA.
[4]Department of Physics and Astronomy, University of Iowa, Iowa City, Iowa, USA.

0094-8276/07/2007GL029986

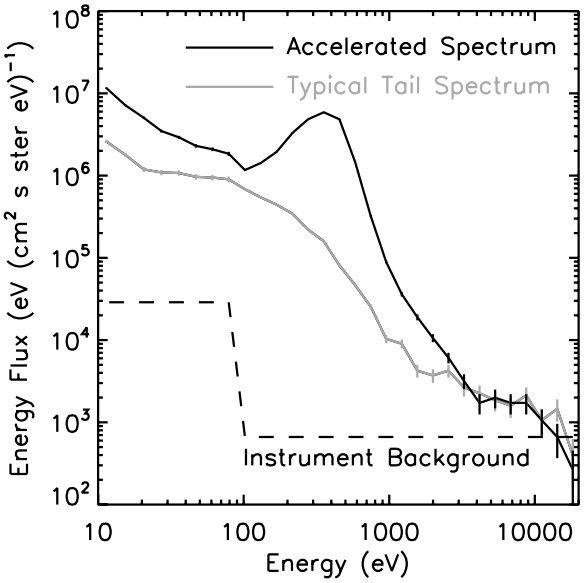

Figure 1. Input spectra for the typical tail (gray) and accelerated (solid) cases.

and Lilensten [1994] developed to model electron transport in the auroral ionosphere of Earth. This code uses the discrete-ordinate method to solve the energy degradation and electron transport problem and uses a multi-stream approach to solve for the electron intensity as a function of energy and altitude.

[7] Necessary modifications to the model of *Lummerzheim and Lilensten* [1994] include incorporating the appropriate CO and CO_2 cross sections for electron impact and using a Martian atmospheric neutral density profile. Currently, the code incorporates over 100 types of elastic and inelastic collisions including dissociations, excitations, and ionizations using cross sections compiled by *Lummerzheim and Lilensten* [1994] for O, O_2, and N_2, and by J. Fox and K. Sung (personal communication, 2001), *Liu and Victor* [1994], and *Itikawa* [2002] for CO and CO_2.

[8] The neutral atmosphere is given by the MTGCM atmosphere of *Bougher et al.* [2000]. The number densities of CO, CO_2, O, O_2, and N_2 are given from 100 to 280 km altitude. For altitudes lower than 100 km, the logarithm of the number densities are linearly extrapolated. Number densities for altitudes above 280 km are extrapolated assuming diffusive equilibrium and an isothermal profile (T = 165 K in this case). We chose a solar moderate case with Mars at perihelion and northern winter solstice. The atmospheric profile is taken at a latitude of 2.5° N and a local time of 02 AM. The exact choice of seasonal and geographic parameters is not of critical importance since our goal is to determine the change in the ionospheric density due to different incident spectra.

[9] The two input energy flux spectra and their error bars are shown in Figure 1. The instrument background level is also shown. Both the typical tail (gray) and accelerated (black) electron spectrum were measured by MGS at 400 km altitude at SZA between 125° and 130° when the magnetic field was nearly radial [*Brain et al.*, 2006]. The accelerated electron spectrum has a large peak at several hundred eV which is absent in the typical tail spectrum. The electrons are mostly isotropic over pitch angles from 0° to 90° [*Brain et al.*, 2006]. The downward particle energy flux for the accelerated spectrum is $\sim 6.0 \times 10^{-3}$ mW m^{-2}, an order of magnitude larger than for the typical case.

3. Model Results

[10] Figure 2 shows the vertical profiles of the ionization rates for CO_2 (dotted) and O (dashed) and the total ionization rate (solid) for the typical (gray) and accelerated (black) cases. Only the CO_2 and O ionization rates are shown since the ionization rates for the other constituents are at least an order of magnitude less at all altitudes. The maximum production rate for the typical spectrum is ~ 1 cm^{-3} s^{-1} and ~ 10 cm^{-3} s^{-1} for the accelerated spectrum.

[11] The electron number density can be computed from the total ion production rate (ignoring dynamics and assuming photochemical equilibrium) from the equation

$$n_e(z) = \left(P(z)/\alpha_{eff}(z)\right)^{1/2}$$

where $P(z)$ is the total ion production rate and $\alpha_{eff}(z)$ is the effective recombination rate. Due to rapid reactions between CO_2, O, and their ions, O_2^+ is the dominant ion in the ionosphere of Mars over the altitudes considered here [*Fox et al.*, 1993, 1996; *Haider*, 1997]. Therefore, α_{eff} is taken to be the dissociative recombination rate of O_2^+ (e.g., *Sheehan and St.-Maurice* [2004]:

$$\alpha = 1.95 \times 10^{-7}(300/T_e)^{0.7}\ \mathrm{cm^3 s^{-1}}\ \text{for}\ T_e < 1200\ \mathrm{K}$$

where T_e is the electron temperature. In the absence of measured nighttime electron temperatures, we assume that the electron temperature is equal to the neutral temperature of 165 K yielding a recombination rate of $\sim 3 \times 10^{-7}$ cm^3 s^{-1}.

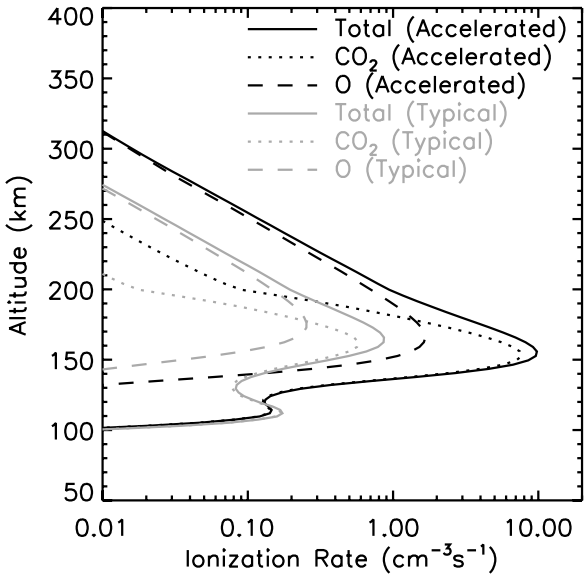

Figure 2. Vertical profiles of the ionization rates for CO_2 (dotted) and O (dashed) and the total ionization rate (solid) for the typical (gray) and accelerated (black) cases.

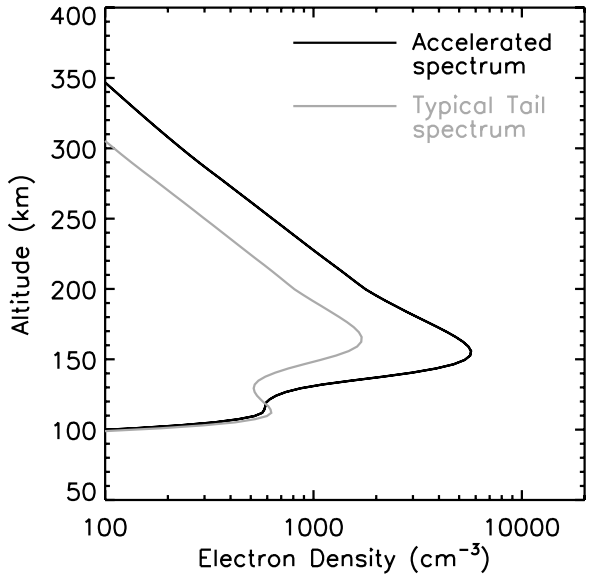

Figure 3. Resulting electron density profiles for typical (gray) and accelerated (solid) incident electron spectra.

[12] Figure 3 shows the electron density profiles resulting from the typical (gray) and accelerated (black) spectra. The maximum electron density (n_e^{max}) for the typical case is 1.7×10^3 cm^{-3} at 166 km altitude; for the accelerated case, it is 5.7×10^3 cm^{-3} at 156 km. The total electron content (TEC) for the typical and accelerated cases are 1.4×10^{14} m^{-2} and 3.5×10^{14} m^{-2}, respectively. The accelerated spectrum increases n_e^{max} by over a factor of 3 while the TEC increases by a factor of 2.5 over that produced by the typical spectrum.

[13] For both cases, a secondary electron peak of 6×10^2 cm^{-3} occurs near 110 km. While a secondary electron density peak produced by solar X-rays has been observed and modeled on the dayside [*Fox et al.*, 1996; *Martinis et al.*, 2003], this is the first time a secondary peak has been modeled due to electron precipitation on the nightside. The electron densities produced by the two input spectra in the vicinity of this peak are nearly the same and appear to be sensitive to ~3 to 10 keV electrons which are observed to have similar fluxes (see Figure 1). All previous calculations of the nightside electron density have only considered precipitating electrons with energies < 1 keV.

4. Comparison with previous work

[14] Table 1 summarizes the main ionospheric parameters derived from our model and compares these to observations and previous modeling results. The n_e^{max} produced by our typical and accelerated spectra bracket those determined at similar SZA by Mars 4 [*Savich et al.*, 1976; *Armand et al.*, 2003] and Viking 1 & 2 [*Zhang et al.*, 1990] (~5×10^3 cm^{-3} in both cases). The altitude of n_e^{max} is in good agreement with the Viking observations of 150 km. Interestingly, the altitude of our secondary peak at 110 km agrees well with the peak altitude from Mars 4 observations. *Zhang et al.* [1990] noted that 60% of the Viking RO measurements on the nightside of Mars yielded no detectable electron density peaks. Since their sensitivity was a few $\times 10^3$ cm^{-3}, the ionospheric density produced by our typical spectrum is consistent with their "zero density" profiles.

[15] Recent nightside observations from the MEX MARSIS Active Ionospheric Sounder (AIS) give typical n_e^{max} of 8×10^3 cm^{-3} and 5×10^4 cm^{-3} over non-magnetic and magnetic regions, respectively [*Kirchner et al.*, 2006, 2007]. The non-magnetic region n_e^{max} is nearly 5 times larger than our typical spectrum value, while the magnetic region number density is nearly 9 times greater that that produced by our accelerated spectrum. Such discrepancies, especially over magnetic regions, could be due to the fact that MGS makes in-situ point measurements of the incident electron flux while MARSIS can receive reflections from a comparatively large area of the ionosphere. Another possibility is that by assuming that the electron temperature is equal to the neutral temperature, we are underestimating the electron density; a larger electron temperature decreases α_{eff} and increases n_e^{max}. Finally, transport processes could play a significant role in maintaining n_e^{max} (e.g., *Fox et al.* [1993]). In particular, over strongly magnetized regions, local dynamo processes may be important in modifying the electron density profile as suggested by *Withers et al.* [2005].

[16] The analytical calculations of *Verigin et al.* [1991], the two-stream model of *Haider et al.* [1992], and the multi-stream method of *Fox et al.* [1993] using the same magnetotail lobe spectrum measured by Phobos 2 yielded n_e^{max} of (7 - 14) $\times 10^3$ cm^{-3}. The peak ion production rates calculated by *Haider et al.* [1992] and *Fox et al.* [1993] were about 30 and 20 cm^{-3} s^{-1}, respectively, compared to ~1 cm^{-3} s^{-1} for our typical case. Their lobe spectrum had an order of magnitude larger flux than our typical spectrum between 10 and 300 eV. Later, using an analytical yield spectrum approach and a precipitating solar wind electron spectrum from 10 to 1000 eV observed by MGS, *Haider et al.* [2002] computed a peak ionization rate of ~6 cm^{-3} s^{-1}

Table 1. Summary of Nightside Observations and Models

	n_e^{max}, (cm^{-3})	Altitude of n_e^{max}, (km)
Typical tail spectrum	1.7×10^3	166
Accelerated spectrum	5.7×10^3	156
Observations		
Mars 4 radio occultation (RO) profile[a]	4.7×10^3	110
Viking 1 & 2 RO profiles (typical)[b]	5×10^3	150
MARSIS Active Ionospheric Sounder[c]		
non-magnetic regions (typical)	8×10^3	175
magnetic regions (typical)	5×10^4	127
Previous models		
Magnetotail lobe spectrum[d]	7×10^3	165
Magnetotail lobe spectrum[e]	1.2×10^4	158
Plasma sheet spectrume[e]	1.7×10^4	144
20 eV Maxwellian (lobe)[f]	1.4×10^4	172
180 eV Gaussian (plasma sheet)[f]	1.9×10^4	159
Solar wind spectrum[g]	5×10^3	140

[a]From *Savich et al.* [1976], *Armand et al.* [2003].
[b]From *Zhang et al.* [1990].
[c]From *Kirchner et al.* [2006, 2007].
[d]From *Verigin et al.* [1991].
[e]From *Haider et al.* [1992].
[f]From *Fox et al.* [1993].
[g]From *Haider et al.* [2002].

and an n_e^{max} of 5×10^3 cm^{-3}. Their solar wind spectrum was 3 times smaller than the lobe spectrum used earlier, yet still ~3 times larger than our typical spectrum.

[17] The plasma sheet spectrum used by *Haider et al.* [1992] and *Fox et al.* [1993] was similar to our accelerated spectrum from 300 to 500 eV (their highest energy); between 100 to 300 eV the plasma sheet flux was about two times larger than our accelerated flux. *Haider et al.* [1992] and *Fox et al.* [1993] calculated production rates of 65 cm^{-3} s^{-1} and 52 cm^{-3} s^{-1}, respectively, about 5 to 6 times larger than our accelerated case resulting in n_e^{max} ~3 times larger than ours. While much of this discrepancy may be due to the difference in flux levels or refinements in electron impact cross sections over the past 10 years, we suspect that differences in the neutral atmospheric profile may play a role as well. Earlier works used profiles from the MTGCM of *Bougher et al.* [1990] under equinox conditions with a median Sun-Mars distance. In contrast, we use an updated MTGCM profile [*Bougher et al.*, 2000] at northern winter solstice and perihelion. Under these conditions the upper atmosphere is warmer [*Bougher et al.*, 1990], resulting in a larger scale height. Electron impact ionization will then occur over a larger altitude range in the upper atmosphere decreasing the peak ionization rate.

5. Conclusion

[18] We have shown that precipitation of recently observed accelerated electron spectra can increase the modeled n_e^{max} and TEC in the nighttime ionosphere of Mars by a factor of three as compared to that produced by typical tail spectra. This should not be regarded as an upper limit since, as noted by *Brain et al.* [2006], the downgoing particle energy flux has been observed to be up to 40 times greater than that of the accelerated spectrum used here. Also, our model shows the presence of a secondary electron density peak at 110 km altitude due to the precipitation of >1 keV electrons that has not been reported in previous nightside modeling efforts. Unlike earlier high altitude (~10,000 km) observations by Phobos 2 [*Verigin et al.*, 1991], the spectra used here were measured by MGS at 400 km altitude where the magnetic field was nearly radial. Therefore, we can be assured that these electrons will interact with the nightside atmosphere.

[19] The small latitudinal extent of cusps where accelerated spectra are observed suggests that the regions of increased ionization should be localized and patchy. In the example shown by *Brain et al.* [2006] (from which our input spectra were taken), the latitudinal width of the region of accelerated electrons was ~200 km at the 400 km altitude of MGS. Due to the focusing effect of strong magnetic gradients associated with crustal sources, this width should be regarded as an upper limit on the scale size of the region of increased ionization. Radio occultation measurements by MGS [*Withers et al.*, 2005] and ionospheric soundings from MEX MARSIS [*Duru et al.*, 2006] have likewise revealed the presence of significant small scale ionospheric structure associated with strong crustal fields.

[20] Calculations of ionospheric electron density have important implications for subsurface radar soundings from orbit. The penetration depth to which soundings can reach is inversely proportional to the signal frequency. To traverse the ionosphere, this frequency must be above the ionospheric electron plasma frequency which is determined by n_e^{max}. Increased ionospheric densities lead to decreased penetration depths. Finally, most previous work addressing how radio waves propagate through ionospheres assumes horizontal uniformity of the ionospheric density (e.g., *Armand et al.* [2003]). This work shows that such an assumption is not valid in the nightside ionosphere of Mars.

[21] **Acknowledgments.** The work at UCB was supported in part by NASA grant NNX06AD97G. SWB was supported by NASA grant NNG04GJ94G. DLK was supported by NASA via contract 1224107 administered by JPL.

References

Acuña, M. H., et al. (2001), Magnetic field of Mars: Summary of results from the aerobraking and mapping orbits, *J. Geophys. Res.*, *106*(E10), 23,403–23,418.

Armand, N. A., V. M. Sitnov, and T. Hagfors (2003), Distortion of radar pulses by the Martian ionosphere, *Radio Sci.*, *38*(5), 1090, doi:10.1029/2002RS002849.

Bougher, S. W., R. G. Roble, E. C. Ridley, and R. E. Dickinson (1990), The Mars thermosphere: 2. General circulation with coupled dynamics and composition, *J. Geophys. Res.*, *95*(B9), 14,811–14,827.

Bougher, S. W., S. Engel, R. G. Roble, and B. Foster (2000), Comparative terrestrial planet thermospheres: 3. Solar cycle variation of global structure and winds at solstices, *J. Geophys. Res.*, *105*(E7), 17,669–17,692.

Brain, D. A., et al. (2006), On the origin of aurorae on Mars, *Geophys. Res. Lett.*, *33*, L01201, doi:10.1029/2005GL024782.

Duru, F., D. A. Gurnett, T. F. Averkamp, D. L. Kirchner, R. L. Huff, A. M. Persoon, J. J. Plaut, and G. Picardi (2006), Magnetically controlled structures in the ionosphere of Mars, *J. Geophys. Res.*, *111*, A12204, doi:10.1029/2006JA011975.

Fox, J. L., J. F. Brannon, and H. S. Porter (1993), Upper limits to the nightside ionosphere of Mars, *Geophys. Res. Lett.*, *20*(13), 1342–1391.

Fox, J. L., P. Zhou, and S. W. Bougher (1996), The Martian thermosphere/ionosphere at high and low solar activities, *Adv. Space Res.*, *17*(11), 203–218.

Gurnett, D. A., et al. (2005), Radar soundings of the ionosphere of Mars, *Science*, *310*(5756), 1929–1933, doi:10.1126/science.1121868.

Haider, S. A. (1997), Chemistry of the nightside ionosphere of Mars, *J. Geophys. Res.*, *102*(A1), 407–417.

Haider, S. A., J. Kim, A. F. Nagy, C. N. Keller, M. I. Verigin, K. I. Gringauz, N. M. Shutte, K. Szego, and P. Kiraly (1992), Calculated ionization rates, ion densities, and airglow emission rates due to precipitating electrons in the nightside ionosphere of Mars, *J. Geophys. Res.*, *97*(A7), 10,637–10,641.

Haider, S. A., S. P. Seth, E. Kallio, and K. I. Oyama (2002), Solar EUV and electron-proton-hydrogen atom-produced ionosphere on Mars: Comparative studies of particle fluxes and ion production rates due to different sources, *Icarus*, *159*, 18–30.

Itikawa, Y. (2002), Cross sections for electron collisions with carbon dioxide, *J. Phys. Chem. Ref. Data*, *31*(3), 749–767.

Kirchner, D. L., D. A. Gurnett, A. Safaeinili, D. D. Morgan, R. L. Huff, J. J. Plaut, and G. Picardi (2006), Radar sounding observations of the nightside Martian ionosphere, *Geophys. Res. Abs.*, *8*, 05224.

Kirchner, D. L., D. A. Gurnett, J. D. Winningham, A. Safaeinili, J. J. Plaut, and G. Picardi (2007), Auroral ionization patches on the nightside of Mars, *Geophys. Res. Abs.*, *9*, 04627.

Leblanc, F., O. Witasse, J. Winningham, D. Brain, J. Lilensten, P.-L. Blelly, R. A. Frahm, J. S. Halekas, and J.-L. Bertaux (2006), Origins of the Martian aurora observed by SPICAM on board Mars Express, *J. Geophys. Res.*, *111*, A09313, doi:10.1029/2006JA011763.

Liu, W., and G. A. Victor (1994), Electron energy deposition in carbon monoxide gas, *Ap. J.*, *435*(2), 909–919.

Lummerzheim, D., and J. Lilensten (1994), Electron transport and energy degradation in the ionosphere: Evaluation of the numerical solution, comparison with laboratory experiments and auroral observations, *Ann. Geophys.*, *12*(10), 1039–1051.

Lundin, R., et al. (2006), Plasma acceleration above Martian magnetic anomalies, *Science*, *311*(5763), 980–983, doi:10.1126/science.1122071.

Martinis, C. R., J. K. Wilson, and M. J. Mendillo (2003), Modeling day-to-day ionospheric variability on Mars, *J. Geophys. Res.*, *108*(A10), 1383, doi:10.1029/2003JA009973.

Mitchell, D. L., R. P. Lin, C. Mazelle, H. Rème, P. A. Cloutier, J. E. P. Connerney, M. H. Acuña, and N. F. Ness (2001), Probing Mars' crustal

magnetic field and ionosphere with the MGS Electron Reflectometer, *J. Geophys. Res.*, *106*(E10), 23,419–23,427.

Savich, N. A., V. A. Samovol, M. B. Vasilyev, A. S. Vyshlov, L.N. Samoznaev, A. I. Sidorenko, D. Y. Shtern (1976), The nighttime ionosphere of Mars from Mars-4 and Mars-5 radio occultation dual-frequency measurements, in *Solar-Wind Interaction with the Planets Mercury, Venus, and Mars*, edited by N. F. Ness, pp. 41–46, NASA, NASA SP-397.

Sheehan, C. H., and J.-P. St.-Maurice (2004), Dissociative recombination of N_2^+, O_2^+, and NO^+: Rate coefficients for ground state and vibrationally excited ions, *J. Geophys. Res.*, *109*, A03302, doi:10.1029/2003JA010132.

Verigin, M. I., K. I. Gringauz, N. M. Shutte, S. A. Haider, K. Szego, P. Kiraly, A. F. Nagy, and T. I. Gombosi (1991), On the possible source of the ionization in the nighttime Martian ionosphere: 1. Phobos 2 HARP electron spectrometer measurements, *J. Geophys. Res.*, *96*(A11), 19,307–19,313.

Withers, P., M. Mendillo, H. Rishbeth, and D. P. Hinson, A. J. Arkani-Hamed (2005), Ionospheric characteristics above Martian crustal magnetic anomalies, *Geophys. Res. Lett.*, *32*, L16204, doi:10.1029/2005GL023483.

Zhang, M. H. G., J. G. Luhmann, and A. J. Kliore (1990), An observational study of the nightside ionospheres of Mars and Venus with radio occultation methods, *J. Geophys. Res.*, *95*(A10), 17,095–17,102.

S. W. Bougher, Department of Atmospheric, Oceanic and Space Sciences, University of Michigan, Ann Arbor, MI 48109-2143, USA.

D. A. Brain, M. O. Fillingim, J. S. Halekas, R. J. Lillis, R. P. Lin, D. L. Mitchell, and L. M. Peticolas, Space Sciences Laboratory, University of California, Berkeley, CA 94720-7450, USA. (matt@ssl.berkeley.edu)

D. L. Kirchner, Department of Physics and Astronomy, University of Iowa, Iowa City, IA 52242-1479, USA.

D. Lummerzheim, Geophysical Institute, University of Alaska, Fairbanks, AK 99775-7320, USA.